Some New Operational Modes and Parameters of Stress Relaxation for the Viscoelastic Characterization of Solid Polymers. III. The Area Ratio Mode and the Intrinsic "Strain–Clock" Function

V. N. Kytopoulos, G. D. Bourkas, E. Sideridis

National Technical University of Athens, Department of Engineering Science, Section of Mechanics, 5 Heroes of Polytechnion Avenue, GR-157 73 Athens, Greece

Received 18 July 2001; accepted 13 February 2002

ABSTRACT: The introduced area ratio mode of operation with its corresponding parameters seems to have a fairly high sensitivity to the viscoelastic response of the solid polymer. This appeared from the fact that a good distinction among the linear viscoelastic, the nonlinear viscoelastic, and the viscoplastic ranges of behavior can be made. By using a relevant rheological modeling and its corresponding algorithmical approach, in the case of isotactic polypropylene, this material can be characterized as a morphological three-phase material consisting of an intraspherulitic crystalline, an amorphous phase, and a interspherulitic *para*-crystalline phase. In this sense, the material was simulated using two models: the Poynting–Thomson and the Maxwell–Wierchert, from where a good response of the material to the first model appeared. The so-called intrinsic "strain–clock" function and its corresponding coefficient of strength of nonlinear viscoelastic behavior, which were relieved by the experimental data, seem to be some powerful and very practical "tools" that can give a proven suplementary characterization of the material. Finally, by this intrinsic function, the existence of permanent internal stresses, was confirmed, in an indirect way, which was mentioned in part II of this study. © 2002 Wiley Periodicals, Inc. J Appl Polym Sci 87: 149–158, 2003

Key words: poly(propylene) (PP); relaxation; modeling; viscoelastic properties; modulus

INTRODUCTION

The need for finding new ways and parameters for a more practical but also a detailed as possible description (characterization) of the viscoelastic behavior of a polymeric solid is known and obvious, and its important significance was described, in general, in parts I and II of this study. In these two parts, it was shown that the principles of the introduced operational modes and parameters, such as, for example, the "virtual modulus" and the "intrinsic time–strain clock" function, were developed based on some already-known very general principles, like those concerning the "vertical shift" but also the relaxation moduli. In the present part III of this investigation, further attempts were made to introduce and prove a new mode of operation, the principle of which is not based on any of the previously known general assumptions presented in parts I and II of this study. In this way, some corresponding parameters arise which can describe and interpret, in some detail, some viscoelastic characteristics of the polymeric solids. Of course, various basic known "facts," which were used in the mathematical modeling and the algorithmic approaches of this study, were based on the Poynting–Thomson body (model), which belongs to the so-called third-generation rheological bodies[1] and which was first proposed by Poynting and Thomson in 1929 to explain the behavior of glass-fibers. (Later, Zener named this body a "standard linear solid".) Based on the above-mentioned body but also on a "second-generation body,"[1] that is, the so-called Maxwell body expressed by a multielemental model, we tried to approach the real body (polymeric solid), which, in our case, was isotactic polypropylene (iPP).

THEORETICAL CONSIDERATIONS AND MODELING

Principle of the area ratio mode

Taking into consideration the scheme in Figure 1, we can obtain the general relationship

$$\frac{\sigma_0 t_r - \int_0^{t_r} \sigma(t)\, dt}{\sigma_0 t_r} + \frac{\int_0^{t_r} \sigma(t)\, dt}{\sigma_0 t_r} = 1 \qquad (1)$$

Correspondence to: V. N. Kytopoulos.

Journal of Applied Polymer Science, Vol. 87, 149–158 (2003)

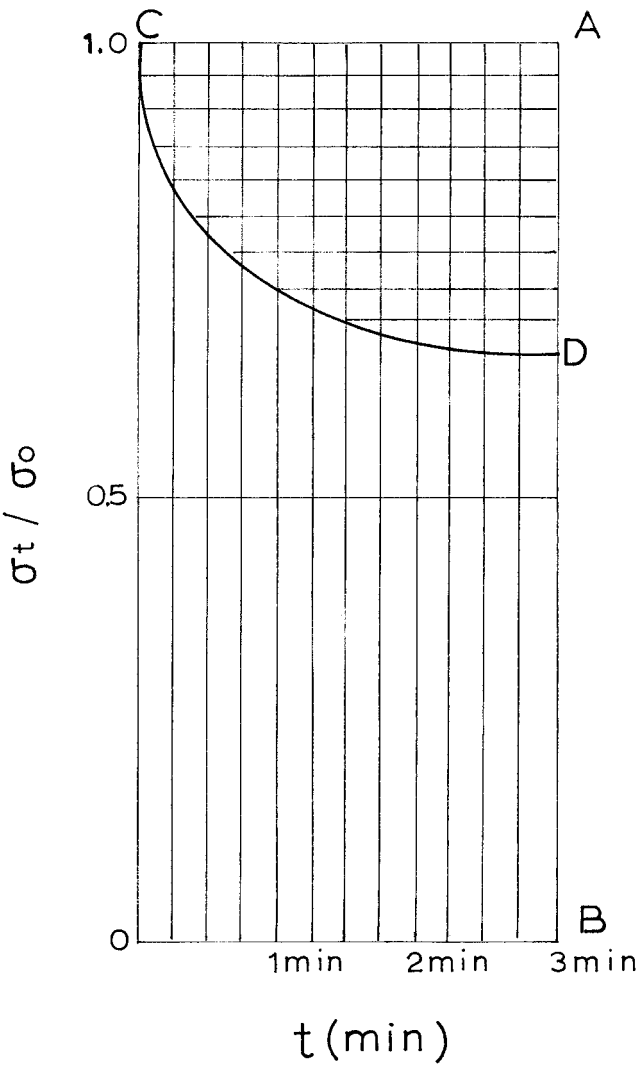

Figure 1 Scheme of the stress relaxation "areas ratio" operative mode.

$$\frac{\text{Area } CAD}{\text{Area } CABO} = \frac{\sigma_0 tr - \int_0^t \sigma(t)\, dt}{\sigma_0 tr}$$

$$\frac{\text{Area } CDBO}{\text{Area } CABO} = \frac{\int_0^{t_r} \sigma(t)\, dt}{\sigma_0 t_r} \tag{1a}$$

where t_r is a reference observation time.

Now, taking into the consideration this relation, we can introduce, formally, the following specific parameters:

$$R_e + \frac{1}{R_I} = 1 \tag{1a}$$

from which

$$R_e = \frac{\sigma_0 t_r - \int_0^{t_r} \sigma(t)\, dt}{\sigma_0 t_r} \tag{2}$$

and

$$R_i = \frac{\sigma_0 \cdot t_r}{\int_0^{t_r} \sigma(t)\, dt} \tag{3}$$

R_e and R_I are both functions of time t_r and will be defined in the following text.

Relation (1a) reminds one of a similar one in thermodynamics, concerning the Carnot "machine" phenomenon and which can be written as follows:

$$\eta + \frac{1}{T_1/T_2} = 1 \tag{4}$$

where η describes the "machine's" efficiency and the ratio T_1/T_2 expresses, in a certain way, a kind of "thermal gradient" or "potential" of the Carnot phenomenon. Consequently, the relations 1(a) and (4) have some common notions, such as:

When $T_1/T_2 \to \infty$, it must be $\eta \to 1$ and, similarly, when $R_1 \to \infty$, it must be $R_e \to 1$. Also, when $T_1/T_2 \to 1$, it must be $\eta \to 0$ and, similarly, when $R_I \to 1$, it must be $R_e \to 0$.

Now, taking into consideration the above statements, we can make the following formalistic correspondence: $R_e \to \eta$ and $R_I \to T_1/T_2$. In this sense, we can define the parameter R_e as a specific relaxation efficiency (SRE) and R_I as a specific relaxation potential or intensity (SRI).

In other words, relation (1a) could be interpreted as follows: If for a given t_r the relaxation potential (intensity) is "infinite," then the relaxation efficiency tends to be a maximum equal to 1 (unit), meaning that we have a perfect 100% "output" of events, that is, an "infinite" number of molecular rearrangements can take place. But if the relaxation potential is a minimum of 1 (unit), then the relaxation efficiency becomes "zero," which means that no molecular rearrangements can take place.

Yet, relation (1a) can be written as $R_e + R_d = 1$, where R_d is now a so-called specific "deficiency" of the relaxation phenomenon. We can make some further interpretations by putting $\tilde{R}_e = R_e/t_r$ as an equivalent (specific) efficiency rate and $\tilde{R}_I = R_I/t_r$ as an equiva-

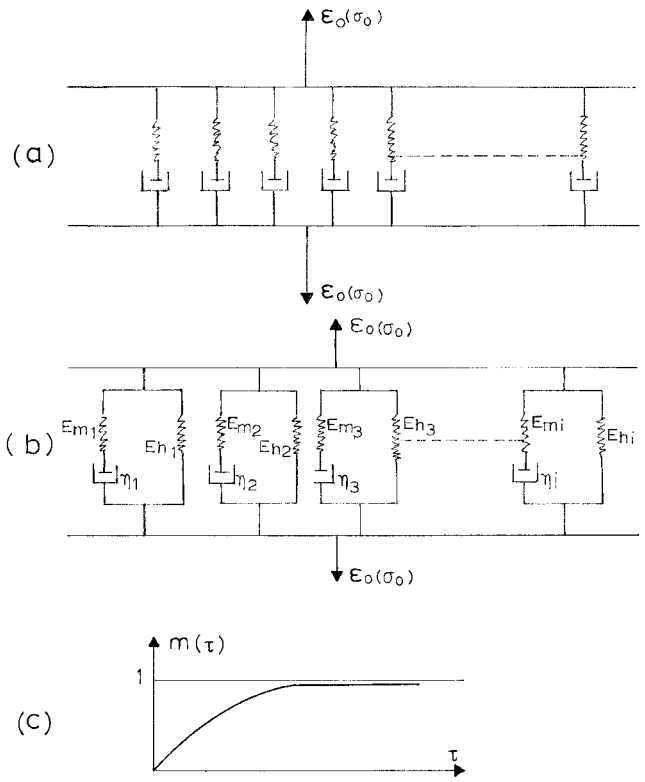

Figure 2 (a) Scheme of the Maxwell–Wierhert body (multielemental Maxwell model). (b) Scheme of the general Poynting–Thomson body (multielemental standard solid model). (c) Scheme of the effective Maxwelian "step function."

lent specific intensity rate. In this case, the general eq. (1a) becomes

$$t_r\tilde{R}_e + \frac{1}{t_r}\frac{1}{\tilde{R}_I} = 1 \quad \text{or} \quad t_r\tilde{R}_e + \frac{1}{t_r}t_i = 1 \tag{5}$$

where $\tilde{t}_i = 1/\tilde{R}_I$ is now a operational "specific relaxation time," during which, for a given potential or intensity of molecular motions, only certain molecular rearrangements take place. From the above definitions, it can be deduced that both $R_e(\tilde{R}_e)$ and $R_I(\tilde{R}_I)$ are a kind of effective measure for the stress-relaxation rate of the polymeric solid.

Basic functional relations

As was already mentioned and is well known, the behavior of a material in stress relaxation is approached better by a multielemental model with Maxwell elements in parallel formation [Fig. 2(a)]. Thus, a Maxwell element in relaxation is given by

$$\eta\dot{\varepsilon}_c(t, \tau) = \sigma_0(t) \tag{6}$$

where $\dot{\varepsilon}_c$ is the strain rate (creep rate); $\sigma_0(t)$, the time function of stress with the initial value σ_0, which corresponds to the initial constant deformation ε_0; and $\tau_0 = \eta/E$, the characteristic relaxation time. Therefore, for a given observation reference time t_r, we have

$$\eta\int_0^{t_r}\dot{\varepsilon}(t, \tau)dt = \int_0^{t_r}\sigma(t)\,dt = \eta[\varepsilon_c^{(r)}(\tau_0) - \varepsilon_c^{(0)}(\tau_0)] = \eta\varepsilon_c^{(r)}(\tau_0) \tag{6a}$$

where $\varepsilon_c^{(r)}(\tau_0)$ is the reference deformation for $t = t_r$ and $\varepsilon_c^{(0)}(\tau_0) = 0$ for $t = 0$. Considering relation (2) and taking into consideration eq. (6a), we have

$$R_e = \frac{\sigma_0 t_r - \eta\varepsilon_c^{(r)}(\tau_0)}{\sigma_0 t_r} = \frac{E\varepsilon_0 t_r - \eta\varepsilon_c^{(r)}(\tau_0)}{E\varepsilon_0 t_r}$$

$$= \frac{\varepsilon_0 - \left(\frac{\eta}{E}\right)\left[\frac{\varepsilon_c^{(r)}(\tau_0)}{t_r}\right]}{\varepsilon_0} = \frac{\varepsilon_0 - \tau_0\tilde{\varepsilon}_c}{\varepsilon_0} \tag{6b}$$

where $\tau_0\tilde{\varepsilon}_c \le \varepsilon_0$, and $\tilde{\varepsilon}_c$ is an average effective deformation with $\tilde{\varepsilon}_c = \varepsilon_c^{(r)}(\tau_0)/t_r$.

For a model with several "n" parallel Maxwell elements, that is, for a general Maxwell model or a Maxwell–Wiechert body,[2] as shown in Figure 2(a), we obtain

$$\sigma(t) = \sum_{i=1}^{n}\sigma_i(t) = \sum_{i=1}^{n}\eta_i\dot{\varepsilon}_{ci}(t, \tau_{0i}) \tag{6c}$$

and after integration

$$\int_0^{t_r}\sigma(t)\,dt = \sum_{i=1}^{n}\int_0^{t_r}\eta_i\dot{\varepsilon}_{ci}(t, \tau_{0i}) = \sum_{i=1}^{n}\eta_i\varepsilon_{ci}^{(r)}(\tau_{0i}) \tag{6d}$$

Therefore, relation (6b) gives

$$R_e = \frac{\sum_{i=1}^{n}E_i\varepsilon_0 t_r - \sum_{i=1}^{n}\eta_i\varepsilon_{ci}^{(r)}(\tau_{0i})}{\sum_{i=1}^{n}E_i\varepsilon_0 t_r} = \frac{\varepsilon_0 - \sum_{i=1}^{n}\tilde{\tau}_{0i}\tilde{\varepsilon}_{ci}}{\varepsilon_0} \tag{7}$$

where $\tilde{\tau}_{0i} = \eta_i/\tilde{E}$ is an effective relaxation time, $\tilde{E} = \Sigma_i^n E_i$ is an effective spring modulus, and $\tilde{\varepsilon}_{ci} = \varepsilon_{ci}^{(r)}(\tau_{0i})/t_r$ is an average effective deformation of a Maxwell element. By writing eq. (7) in another form as follows:

$$R_e = \frac{\varepsilon_0 - \sum_{i=1}^{n} \tilde{M}_{0i}}{\varepsilon_0} = \frac{\varepsilon_0 - \tilde{\tilde{M}}_0}{\varepsilon_0} \tag{8}$$

we can define $\tilde{M}_{0i} = \tilde{\tau}_{0i}\tilde{\varepsilon}_{ci}$ as an effective Maxwell element and $\tilde{\tilde{M}}_0$ as an effective Maxwell body. Expression (3) takes now the form

$$R_I = \frac{\varepsilon_0}{\sum_{i=1}^{n} \tilde{\tau}_{0i}\tilde{\varepsilon}_{ci}} = \frac{\varepsilon_0}{\sum_{i=1}^{n} \tilde{M}_{0i}} = \frac{\varepsilon_0}{\tilde{\tilde{M}}_0} \tag{8a}$$

Next, the analytical expression for the effective Maxwell element $\tilde{M}_{0i}$ can be determined by

$$\sigma_i(t) = E_i\varepsilon_0 \cdot e^{-t_r/\tau_{0i}}$$

which, by integration, gives

$$\frac{1}{\eta_i}\int_0^{t_r} \sigma_i(t)\, dt = \frac{-E_i\varepsilon_0\tau_{0i}[e^{-t/\tau_{0i}}]_0^{t_r}}{\eta_i}$$

$$= \frac{E_i\varepsilon_0\tau_{0i}[1 - e^{-t_r/\tau_{0i}}]}{\eta_i} = \varepsilon_{ci}^{(\tau)}(\tau_{0i}) \tag{9}$$

which leads to

$$\varepsilon_{ci}^{(r)}(\tau_{0i}) = \varepsilon_0[1 - e^{-t_r/\tau_{0i}}] \tag{9a}$$

Therefore,

$$\tilde{M}_{0i} = \tilde{\tau}_{0i}\tilde{\varepsilon}_{ci} = \varepsilon_0[1 - e^{-t/\tau_{0i}}]\,\frac{\tilde{\tau}_{0i}}{t_r},$$

$$\text{where} \quad \tilde{\tau}_{0i} = \frac{\eta_i}{\tilde{E}} = \tau_{0i}\frac{E_i}{\tilde{E}} = \tau_{0i}\tilde{\tilde{E}}_i \tag{9b}$$

Thus, for the effective Maxwell element, we have the general expression

$$\tilde{M}_{0i} = \tilde{m}_{0i}\tilde{\tilde{E}}_i \tag{9c}$$

with

$$\tilde{m}_{0i} = \varepsilon_0[1 - e^{-t/\tau_{0i}}]\,\frac{\tau_{0i}}{t_r} \tag{9d}$$

where $\tilde{m}_{0i}$ is an effective Maxwell relaxation unit, and $\tilde{\tilde{E}}_i$, an effective "Maxwellian" spring distribution parameter.

For a model with infinite Maxwell elements, where the distribution of the elements with the corresponding relaxation time becomes continuous, the following expression can be written:

$$\tilde{\tilde{M}}_0 = \lim_{n\to\infty} \sum_{i=1}^{n} \tilde{M}_{0i} = \frac{\varepsilon_0}{t_r}\int_0^{\infty} [1 - e^{-t_r/\tau}]\tau g(\tau)\, d\tau \tag{10}$$

where the Maxwellian spring parameter $\tilde{\tilde{E}}_i$ is replaced by a density or weighting function $g(\tau)d\tau$, which defines the distribution or the concentration of the Maxwell elemental units $m(\tau) = (1 - e^{-t_r/\tau})\tau$ with relaxation times between τ and $\tau + d\tau$. With this definition, eq. (10) for the effective Maxwell body gives

$$\tilde{\tilde{M}}_0 = \frac{\varepsilon_0}{t_r}\int_0^{\infty} m(\tau)g(\tau)\, d\tau \tag{10a}$$

Now, we apply to the above relations the Alfrey approximation procedure, which means that we must have the step function

$$\text{for} \quad \tau > t_r, \quad m(\tau) \cong 1$$

$$\tau < t_r, \quad m(\tau) \cong 0 \tag{10b}$$

The above approximation is valid due to the shape of $m(\tau)$ [Fig. 2(c)], because it can be seen that

$$m(\tau = 0) = 0 \quad \text{and} \quad m(\tau \to \infty) = 1 \tag{10c}$$

Therefore, after application of Alfrey's approximation, by relation (10a), we have

$$\tilde{\tilde{M}}_0 \cong \frac{\varepsilon_0}{t_r}\int_{t_r}^{\infty} g(\tau)\, d\tau = \frac{\varepsilon_0}{t_r}\tilde{g}(t_r) \tag{11}$$

In the first instance in the above integral, we can make two kinds of approximations. It is known that the relaxation spectrum can be often approximated by some relevant "box"-type distributions similar to those given in refs. 3 and 4 or, more generally, to those discussed in part I of this study. Thus, we would not make considerable errors if we would assume such a distribution for the function $g(\tau)$. Then, for conveniently "small" times t_r, we can assume, with some sufficient approximation,

$$\int_0^{\infty} g(\tau)\, d\tau \cong \int_0^{t_r} g(\tau)\, d\tau + \int_{t_r}^{\tau<\infty} g(\tau)$$

$$\approx \int_{t_r}^{\tau<\infty} g(\tau)\, d\tau = \tilde{g}(t_r) \approx \text{const} = \tilde{C} \tag{11a}$$

that is, the integral must change very slowly with the observation time t_r. The second kind of approximation is simply to assume that $\tilde{g}(t_r)$ is not constant and, therefore, $\tilde{g}(t_r) = f(t_r)$, that is, it is a much stronger function of t_r. Under these conditions, the relations (8a), (11), and (11a) give

$$R_d = 1/R_I = \frac{\tilde{g}(t_r)}{t_r} \quad \text{or} \quad \frac{1}{\tilde{R}_I} = \tilde{g}(t_r) = \tilde{t}_i \qquad (12)$$

with

$$\tilde{g}_0(t_r) = f(t_r) \quad \text{or} \quad \tilde{g}(t_r) = \tilde{C}$$

Analogous relationships can be obtained for R_e and $\tilde{R}_e$ as well from relation (8).

General Poynting–Thomson-type model (body)

This general body model is constructed by several Poynting–Thomson parallel units, where a Poynting–Thomson unit is constructed by a Maxwell element and a Hookean spring in parallel [see Fig. 2(b)]. For a Poynting–Thomson unit in relaxation, it can be proved[1] that

$$\sigma_i(t)\sigma_{ih}(0) + \sigma_{im}(0)e^{-t/\tau_{0i}} \qquad (13)$$

where $\sigma_{ih}(0)$ is the initial stress of spring "h" ("Hookean" one), and $\sigma_{im}(0)$, the initial stress of spring "m" ("Maxwellian" one). The elements of this Poynting–Thomson model may be strain-dependent, having a general nonlinear type model.

Following the same procedure as in the previous paragraph by taking into consideration the elementary contribution of the dashpot creep deformation and elastic spring one, we have

$$R_e \frac{\sum_{i=1}^{n} [\varepsilon_0(E_{mi} + E_{hi})t_r - \eta_i\varepsilon_{ci}^{(r)} - E_{hi}\varepsilon_0 t_r]}{\sum_{i=1}^{n} \varepsilon_0[E_{hi} + E_{mi}]t_r} \qquad (14)$$

$$\frac{\varepsilon_0 - \left(\sum_{i=1}^{n} \tilde{\tau}_{0i}\tilde{\tilde{\varepsilon}}_{ci} + \sum_{i=1} \tilde{\tilde{E}}_{ih}\varepsilon_0\right)}{\varepsilon_0}$$

where

$$\tilde{\tau}_{0i} \frac{\eta_i}{\sum_{i=1}^{n} \tilde{E}_i}$$

with $\tilde{E}_i\, E_{hi} + E_{mi}$ and $\tilde{\varepsilon}_{ci}\, \varepsilon_{ci}/t_r$, and $\tilde{\tilde{E}}_{ih}\, \mathrm{E_{hi}}/\tilde{\mathrm{E}}_{\mathrm{i}}$ "Hookean" spring distribution parameters. Also, after summation of the elementary dashpot creep and elastic spring deformations, we obtain

$$1/R_I \frac{\sum_{i=1}^{n} [\eta_i\varepsilon_{ci}^{(r)} + E_{hi}\varepsilon_0 t_r]}{\sum_{i=1}^{n} \varepsilon_0(E_{hi} + E_{mi})t_r} \frac{\sum_{i=1}^{n} \int_0^{t_r} \sigma_i(t)\, dt}{\sum_{i=1}^{n} \tilde{E}_i\varepsilon_0 t_r},$$

$$\text{with} \quad \tilde{E}_i E_{hi} + E_{mi} \qquad (15)$$

Integration of the Eq. (13) gives

$$\int_0^{t_r} \sigma_i(t)\, dt\sigma_{hi}(0)t_r + \sigma_{mi}(0)\tau_{0i}[1 - e^{-t_r/\tau_{0i}}] \qquad (16)$$

Comparison of Eqs. (15) and (16) gives

$$\eta_i\varepsilon_{ci}^{(r)}\sigma_{mi}(0)\tau_{0i}[1 - e^{-t_r/\tau_{0i}}] \qquad (17)$$

which leads to

$$\varepsilon_{ci}^{(r)} = E_{mi}\varepsilon_0 \frac{\tau_{0i}}{\eta_i}[1 - e^{-t_r/\tau_{0i}}] = \varepsilon_0(1 - e^{-t_r/\tau_{0i}}) \qquad (17a)$$

This relation has the same form with eq. (9a). Therefore, eq. (15) can be modified using the Maxwell effective unit as follows:

$$1/R_I = \sum_{i=1}^{n} \tilde{M}_{0i}/\varepsilon_0 + \sum_{i=1}^{n} \tilde{\tilde{E}}_{hi} \qquad (18)$$

where

$$\tilde{M}_{0i} = \frac{\varepsilon_0}{t_r}[1 - e^{-t_r/\tau_{0i}}]\tau_{0i} \frac{E_{mi}}{\tilde{E}_i} = \tilde{m}_{0i}\tilde{\tilde{E}}_{im}$$

where $\tilde{\tilde{E}}_{im} = \mathrm{E_{mi}}/\tilde{\mathrm{E}}_{\mathrm{i}}$ is an Maxwellian spring distribution parameter.

Thus, for a continuous set of relaxation times τ_{0i} and also for a distribution with an infinite number of effective Maxwell elements and Hookean springs and after applying the same approximation procedures given by eqs. (10) and (11), we obtain from eq. (18), by taking $n \to \infty$,

$$1/R_I = \sum_{i=1}^{\infty} \tilde{M}_{0i}/\varepsilon_0 + \sum_{i=1}^{\infty} \tilde{\tilde{E}}_{hi} = \frac{\tilde{\tilde{M}}_0}{\varepsilon_0} + \int_0^{\infty} g_1(\tau)\, d\tau = \frac{\tilde{g}_0(t_r)}{t_r} + \tilde{g}_1(t_r) \quad (19)$$

and, hence, as in the case of eqs. (12), we have the two basic operational parameters:

$$R_d = 1/R_I = \frac{\tilde{g}_0(t_r)}{t_r} + \tilde{g}_1(t_r) \quad (20)$$

with

$$\tilde{g}_0(t_r) = f_0(t_r) \quad \text{or} \quad \tilde{g}_0(t_r) = \tilde{C}_0$$
$$\text{and} \quad \tilde{g}_1(t_r) = f_1(t_r) \quad \text{or} \quad \tilde{g}_1(t_r) = \tilde{C}_1$$

or

$$\tilde{t}_i = 1/\tilde{R}_I = \tilde{g}_0(t_r) + \tilde{g}_1(t_r)t_r \quad (20a)$$

with

$$\tilde{g}_0(t_r) = f_0(t_r) \quad \text{or} \quad \tilde{g}_0(t_r) = \tilde{C}_0$$
$$\text{and} \quad \tilde{g}_1(t_r) = f_1(t_r) \quad \text{or} \quad \tilde{g}_1(t_r) = \tilde{C}_1$$

where $\tilde{g}_0(t_r)$ and $\tilde{g}_1(t_r)$ have the same notions given for the interpretation of eq. (12). [Analogous relations can be extracted for R_e and $\tilde{R}_e$ as well from eq. (14).]

EXPERIMENTAL

Particular knowledge of certain constructive parameters on every polymer material, other than general properties and definition, is required before the material enters the experimental stages. Some of these parameters, like the melt-flow index, the molecular mass and weight distribution, and the heterogeneity index (M_n, M_w, D) can be found in parts I and II of this study. Isotropic materials were obtained at 150°C from compression-molded sheets with a thickness of 0.30 cm. The sheets were cooled afterward at room temperature. From these sheets, dog-bone specimens were cut which were tested in stress relaxation. All the stress-relaxation experiments were made at room temperature and at a constant strain rate $\approx 10^{-2}$/s using an Instron-type machine.

RESULTS AND DISCUSSION

Figure 3 gives the experimental path of the curve for $\tilde{R}_e$, that is, the equivalent efficiency rate in relation to the loading grade σ_0/σ_Δ, for three materials. In Figure 4 appears the path of the experimental curve for $\tilde{R}_I$, that is, for the equivalent intensity rate, for three materials. From these two figures, we can observe that the curve presents two or even three different slopes, which can be explained by the existence of corresponding two or three basic types of kinetic behavior: the linear elastic, the nonlinear elastic, and the viscoplastic.

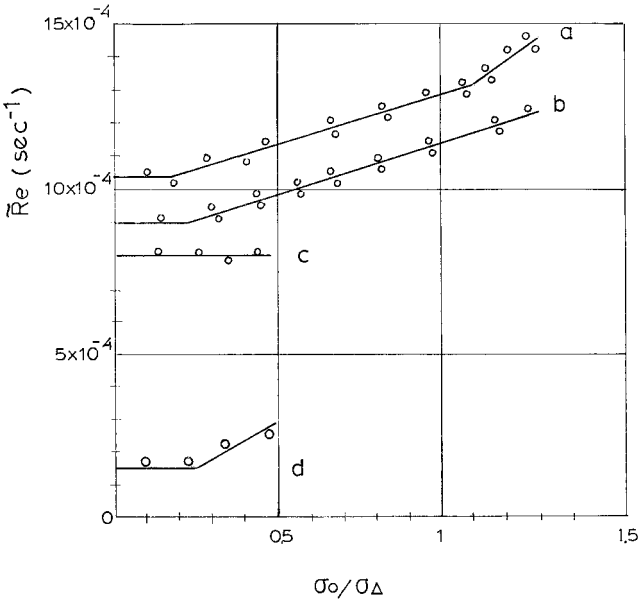

Figure 3 Experimental data of the equivalent specific, efficiency rate, $\tilde{R}_e$, for (a) quenched iPP, (b) annealed iPP, (c) epoxy resin with 70% plasticizer, and (d) Lexan.

Especially for PP, we observe that, for the annealed state, there is a relative "delay" as to the onset of the viscoplastic response, compared with the quenched state. This is consistent with the fact that the annealing process increases the molecular packing density, which tends to inhibit the viscoplastic or viscous flow in the material. In the case of epoxy resin, it appears only as a "linear" behavior for the loading imposed ($\sigma_0/\sigma_\Delta < 0.5$). From the above two figures, we can further argue that Lexan has the lowest relaxation rates, whereas PP has the highest. Plasticized epoxy resin has an intermediate rate, however, closer to that of PP.

In Figures 5 and 6, the "classical," that is, the relative or the reduced stress-relaxation, curves for the same materials are given. Thus, in the first figure, curves only for quenched PP and for various loading grades are given, whereas in the second figure, the curves for all the other materials but for one loading grade are given. Thus, from these figures, the relative weak response of the nonlinear behavior is evident when the loading grades increase, without having the possibility of separation in two or even three ranges of behavior, as became apparent in the curves of Figures 3 and 4 by means of the two "equivalent rates" ($\tilde{R}_I$ and

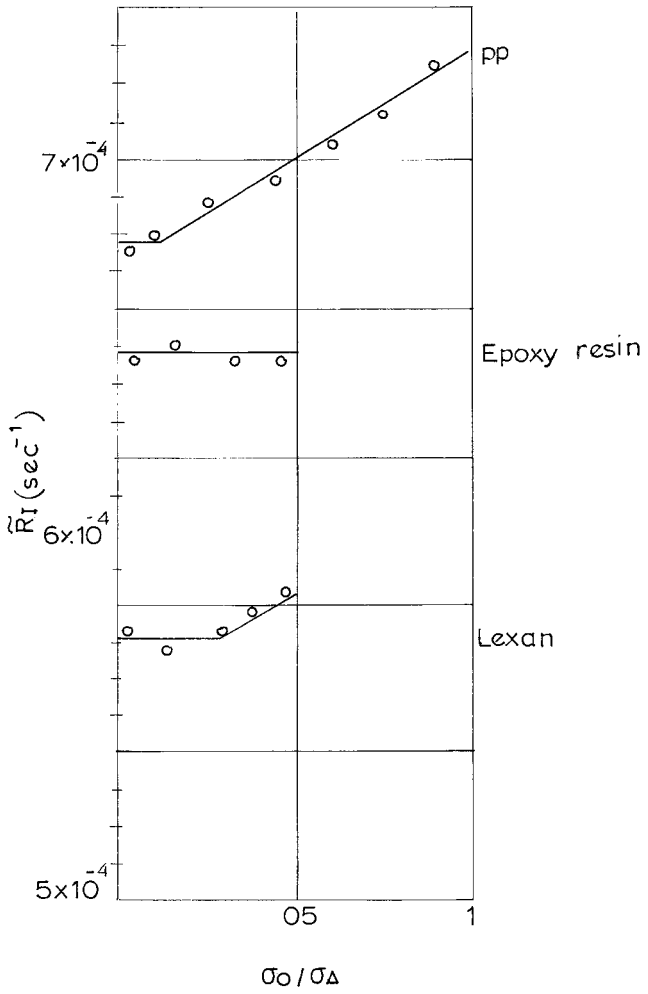

Figure 4 Experimental data of the equivalent specific intensity rate, $\tilde{R}_I$, for (a) iPP, (b) epoxy resin (70% plasticizer), and (c) Lexan.

$\tilde{R}_e$). As stated, this is very well evident for the example in the case of quenched and annealed PP from Figure 3, where we see a clear distinction, whereas from Figure 5, this behavior cannot be extracted. So, we can conclude that the response sensitivity of the "classical" relaxation test (Figs. 5 and 6) is clearly lower than that for the curves of Figure 4 which concern the new technique.

However, some of the most important results of this work are "hidden" in the measurements of Figure 7, where the experimental evidence of eq. (20a), that is, of the proposed "specific relaxation time," $\tilde{t}_i$, in relation to the reference observation time, t_r, for various strains is given. As previously stated, this proposed time can be regarded as a operative time, according to which, for a given potential (intensity) of internal molecular motion, only a certain number of molecular rearrangements and phenomena are conducted. In this context, we observe that the general trend of this evidence is expressed by parallel lines which are shifted to higher operative times as strain increases, which means that a higher number of rearrangements can take place. The slope $\tilde{g}_1(t_r)$ of the lines is constant and we can evaluate it to about 0.85.

The above general trend in Figure 7 becomes more apparent in another manner from Figure 8, where the plot of the experimental curve of eq. (20), that is, the so-called specific "deficiency" R_d, with a satisfactory response is given. In this sense, for $t_r \to \infty$, the experimental curves cut the ordinate at $R_d = \tilde{g}_1 \approx 0.9$. In contrast to these findings, the measurements of Figures 7 and 8 by no means can be approached by the relations (12), which express the Maxwell–Wiechert body and which means that this body cannot be simulated by experiment.

A further result related to the experimental measurements given in Figures 7 and 8 is the above-stated evidence that $\tilde{g}_1(t_r) = \text{const} = \tilde{C}_1 \approx 0.85$, a fact that justifies the approaches made in the relationships given by eqs. (11a), but also the assumptions related to them: that the spectral distributions of the Maxwellian springs and of the whole viscoelastic body are similar, that is, are of box type. In this sense, we may further

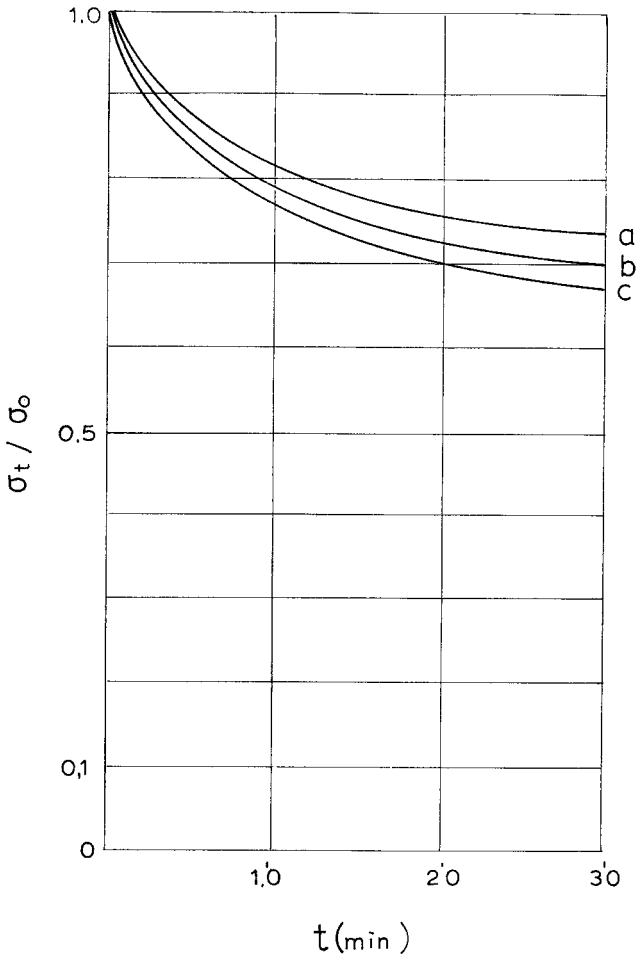

Figure 5 Experimental curves of the (classical) stress-relaxation test for quenched iPP and for some degrees of loading σ_0/σ_Δ: (a) $\sigma_0/\sigma_\Delta \approx 0.2$; (b) $\sigma_0/\sigma_\Delta \approx 0.4$; (c) $\sigma_0/\sigma_\Delta \approx 0.6$.

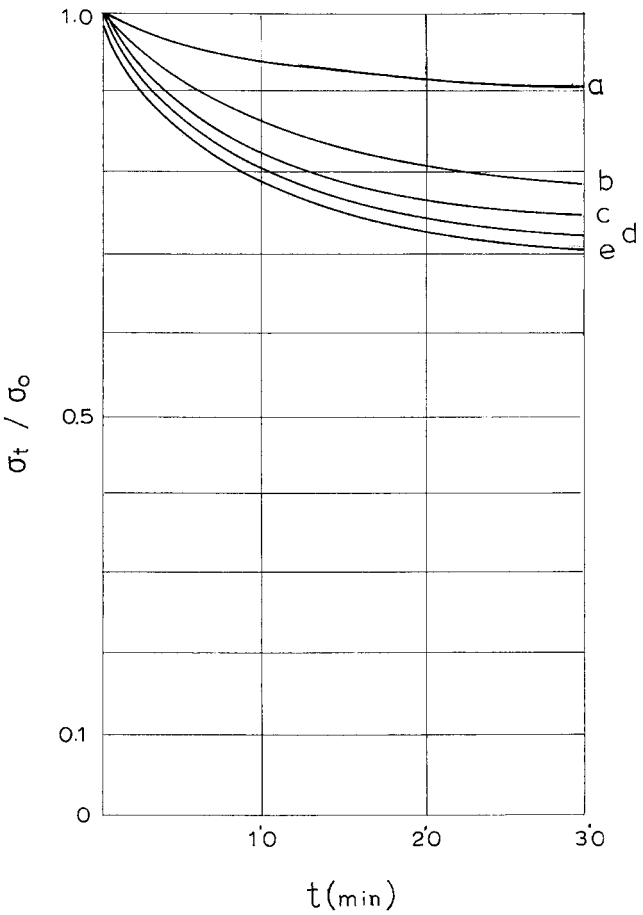

Figure 6 Experimental curves of the (classical) stress-relaxation test for (a) Lexan, (b) epoxy resin (70% plasticizer), (c) annealed iPP, (d) quenched iPP, and (e) stretched up to $\varepsilon_1 \approx 12\%$ and quenched iPP.

judge that, as a further approximation of the condition given in eq. (11a), one can take a very long, but finite time of integration and assume a very slow time-changing function, $\tilde{g}(t_r)$, which leads to the supplementary condition of the relation given by eq. (11a):

$$\int_{t_r}^{\tau=t\gg t_r} g(\tau)\, d\tau = \tilde{g}(t_r) = at_r + \beta \approx \tilde{C} = \text{const} \quad (21)$$

where the slope $|a| \ll 1$. (Relation 21 express a nearly parallel line to the time axis.)

From the above relationship, it can be assumed that the spectral distribution (density) $g(\tau) \approx \beta = \text{const}$ is consistent with the experimental data from parts I and II of this study in the example of iPP, which assumes a spectral box-type distribution for the given experimental observation times. In other words, this means that, if the approximations and assumptions made in the relationships given by eqs. (11a) and (21) are valid, the "partial elastic body" represented only by the Maxwellian and Hookean springs has a similar box-form distribution with those of the whole viscoelastic body.

Concerning the found value for the constant $\tilde{C}_1 \approx 0.85$, we can try to make the following approach: By admiting a relevant average experimental error of $\pm 15\%$, we could put $\tilde{C}_1 \approx 1 \pm 0.15$ as the "true" experimental value. This now leads to the assumption that $\int_0^\infty g_1(\tau)\, d\tau = 1$, which means that the spectral distribution function $g_1(\tau)$ for the Hookean springs could be normalized to unity.[5] In this case, the function $g(\tau)$ might be interpreted in other words as a "probability density" for the "existence" of a Hookean spring during the relaxation time $d\tau$. Normalization to unity means now that, for time starting from zero to "infinity," the probability to "find" any one of these springs is 1, that is, 100%. The above assumptions should not be made for the function $g_0(\tau)$, which gives a distribution density for the Maxwellian springs. This function seems to be strain-dependent [eq. (20) and Fig. 7), that is, it is concerned with the nonlinear behavior of the solid and, as such, it cannot be normalizidet to unity.[5]

Another basic result can be extracted from Figure 7. Thus, from the intersection values of the abscissas with the ordinate axis (for $t_r \to 0$) for various procentual strains ε_0, we found an approximate linear relation which may represent, at the same time, a kind of intrinsic "strain–clock" function:

$$\tilde{t}_i = \tilde{C}_0(\varepsilon_0) \approx \lambda\varepsilon_0 + \beta \quad (22)$$

with $\lambda \approx 2$ and $\beta \approx -3$. This means that for $\varepsilon_0 \to 0$ we must have a "negative" specific relaxation time or a fictive distribution, which may be attributed to the existence of some residual or permanent internal stresses. The existence of such stresses is experimentally confirmed through previously carried out tests, for example, of refs. 6–8, but also through those carried out by the authors in part II of this investigation. Consequently, according to all these, we can say that the results have been confirmed, by an indirect way, of, for example, ref. 6, where the stress-relaxation kinetics is controlled by the initial effective stress $\sigma_0^* = \sigma_0 - \sigma_i$, where σ_i is the internal stress, and σ_0, the actual initial one. In this context for $\sigma_0 = 0$ (or $\varepsilon_0 = 0$), we obtain a "negative" internal stress, which leads to a "negative" (fictive) spectral distribution.

Another significant parameter of eq. (22) is the coefficient λ, which can be seen as a measure of the strength of the nonlinear viscoelastic behavior of this material. Furthermore, from this relation, it can be judged that an intrinsic "strain–clock" must begin to work by giving the nonlinearity strength, λ, and this happens only for $\tilde{C}_2(\varepsilon_0) \geq 0$, that is, for an initial strain ε_0 greater about 1.5%. This value is very close to 1%, which is generally accepted as a conventional one for

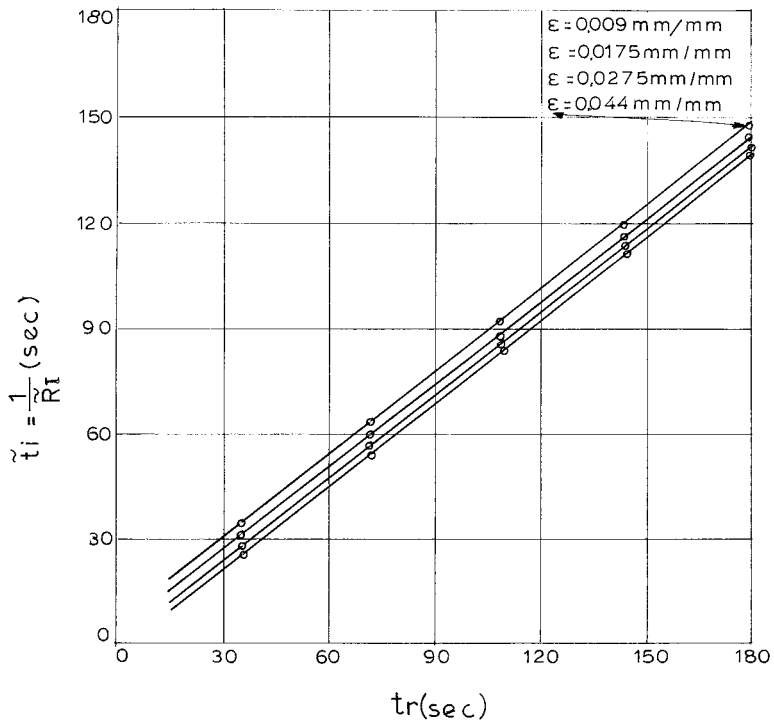

Figure 7 Experimental data plot of the operative specific time, $\tilde{t}_i$, in function of the reference observation time t_r and the applied strain ε_0.

the distinction between linear and nonlinear viscoelastic behavior.[9]

As a general basic result, it can be stated, in closure, we had a rather quite positive experimental response of the Poynting–Thomson model [relations (20) and (20a)] compared to the Maxwell–Wiechert model [relations (12)], which did not respond. Also, this, in general, means that the Poynting–Thomson model better reflects the microstructure and the morphology of PP. In this sense, in this model, the Hookean "soft" springs reflect the amorphous region behavior between the spherulites (interspherulitic connections), regions which remain "stressed," without relaxing at all, while the Maxwellian "hard" springs reflect the behavior of intraspherulitic crystalline regions (folded-chain lamellae), and the dashpot, the behavior of the amorphous intraspherulitic regions. Consequently, it seems that a three-phase model is well simulated and consistent with the dynamic mechanical analysis, showing three maxima of the relaxation spectra: at 60°C, which corresponds to the crystalline phase; at 5°C, which corresponds to the glass transition of the amorphous phase; and at −70°C, which corresponds to the *para*-crystalline phase between spherulites.[10]

CONCLUSIONS

In this article, an effort was made to introduce, in a *modus operandi* way, some effective and practical parameters to characterize the linear and nonlinear viscoelastic behavior of solid polymers using the example of (iPP). Depending on the way used and its corresponding parameters, this effort has shown the following:

(a) The so-called relaxation areas ratio mode, expressed by its corresponding specific rate parameters, seems to be quite sensitive as far as detecting the linear and nonlinear viscoelastic and viscoplastic behavior are concerned.
(b) With the contribution of the previously proposed mode, as well as with the implementation of a relevant, theoretical modeling and its algorithmic approach, it was experimentally proved that iPP behaves quite satisfactorily according to the Poynting–Thomson's-type rheological model. This relative good correlation of experiment and theory is based on the almost "perfect" simulation of this rheological model with the three-phase molecular morphology of iPP.
(c) From the analysis of the experimental data, the evidence of a so-called intrinsic strain-clock function and its corresponding coefficient of strength of nonlinear viscoelastic behavior can be stated.
(d) At the same time, using this function given by the specific relaxation time parameter, a consis-

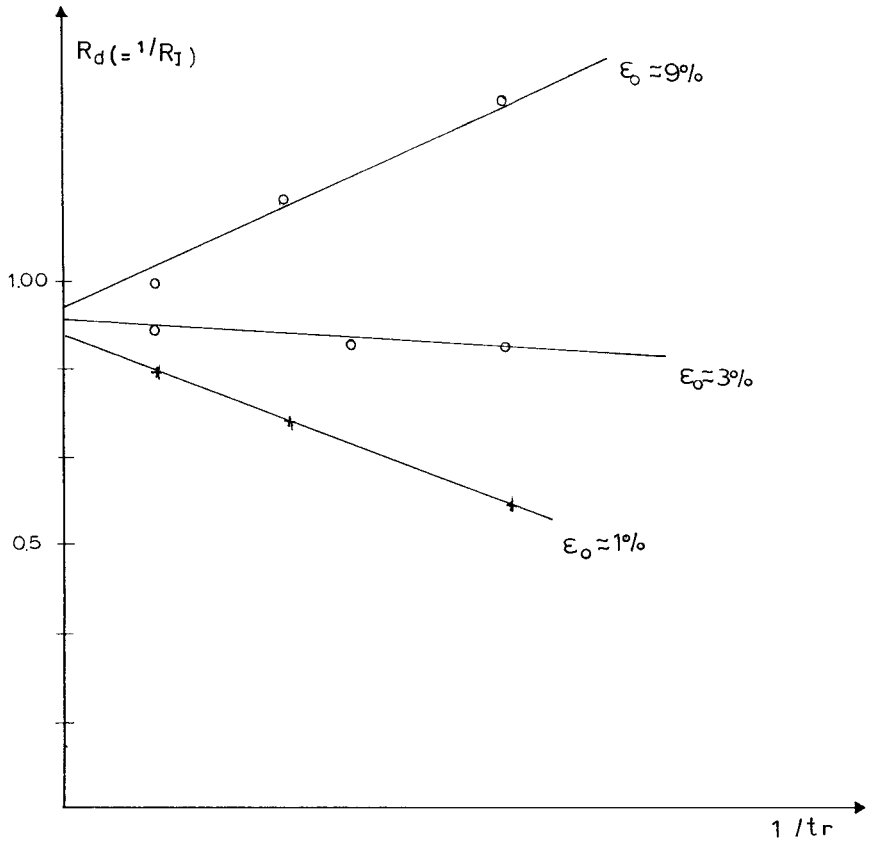

Figure 8 Experimental data plot for the specific deficiency, R_d, in function of applied strain ε_0 and reference observation time t_r.

tency with the evidence of the permanent internal stresses is established.

References

1. Reiner, M. Advanced Rheology; H.K. Lewis: London, 1971.
2. Wiechert, E. Wied Ann Phys 1893, 50, 335, 546.
3. Ferry, J. D. Viscoelastic properties of Polymers; Wiley: New York, London, 1961.
4. Nielsen, L. E. Mechanical Properties of Polymers; Reinhold: New York; Chapmana Hall: London, 1962.
5. Dutta, N. K.; Edward, G. H. J Appl Polym Sci 1997, 66, 1101.
6. Selden, K. J Mater Sci 1979, 14, 312.
7. Kubat, J.; Rigdahl, M.; Selden, R. J Appl Polym Sci 1976, 20, 2799.
8. Kubat, J.; Rigdahl, M. Phys Stat Sol (a) 1976, 35, 173.
9. Ward, I. M.; Onat, E. T. J Mech Phys Solids 1963, 11, 217.
10. Samuels, R. J. In Plastic deformation of Polymers; Peterlin, A., Ed.; Marcel Dekker: New York, 1971.